Published in final edited form as:
J Phys Condens Matter. 2010 February 2; 22(7): 72202. doi:10.1088/0953-8984/22/7/072202.

Fluctuations and interactions of semi-flexible polyelectrolytes in columnar assemblies

D. J. Lee[1,*], **S. Leikin**[2,†], and **A. Wynveen**[3]

[1]Max Planck institute for the physics of complex systems, D-01187, Dresden, Germany

[2]Section of Physical Biochemistry, Eunice Kennedy Shriver National Institute of Child Health and Human Development, National Institutes of Health, DHHS, Bethesda, MD 20892, USA

[3]Institute for Theoretical Physics II: Soft Matter, Heinrich-Heine-University of Düsseldorf, Universitätsstraße 1, D-40225 Düsseldorf, Germany

Abstract

We have developed a statistical theory for columnar aggregates of semi-flexible polyelectrolytes. The applicability of previous, simplified theories was limited to polyelectrolytes with unrealistically high effective charge and, hence, with strongly suppressed thermal undulations. To avoid this problem, we utilized more consistent approximations for short-range image-charge forces and steric confinement, resulting in new predictions for polyelectrolytes with more practically important, lower effective linear charge densities. In the present paper, we focus on aggregates of wormlike chains with uniform surface charge density, although the same basic ideas may also be applied to structured polyelectrolytes. We find that undulations effectively extend the range of electrostatic interactions between polyelectrolytes upon decreasing aggregate density, in qualitative agreement with previous theories. However, in contrast to previous theories, we demonstrate that steric confinement provides the dominant rather than a negligible contribution at higher aggregate densities and significant quantitative corrections at lower densities, resulting in osmotic pressure isotherms that drastically differ from previous predictions.

1. Introduction

Semi-flexible polyelectrolytes play an important role in living systems and they are utilized in many industrial applications [1,2,3]. Their interactions are often studied in condensed columnar assemblies; most notably, examples include DNA [4,5,6,7], actin [4,8,9,10,11], xanthan [5, 12] and some viruses such as TMV [4,13,14]. Aggregation of semi-flexible polyelectrolytes into columnar assemblies is also observed in nature, for instance, DNA in viral capsids [15, 16,17] and actin filaments in microvilli [18]. The aggregation may be brought about by condensing agents [4,19,20] or osmotic pressure [6]. Intermolecular interactions determine physical properties of the aggregates [21] and play a crucial role in such phenomena as packing of meters of DNA inside a cell [22] or ejection of DNA from viruses [17].

It has long been noted that the interplay between interaction forces and undulations may be important for the physics of assemblies of semi-flexible polymers [23,24,25]. An early model of DNA aggregates approximated this interplay by treating a DNA molecule as a flexible chain

*domolee@hotmail.com
†leikins@mail.nih.gov

[1]L. D. Landau, E. M. Lifshitz, *Statistical Physics* (Pergamon, Oxford, 1969)

[2]Feynman, R. P., and Hibbs, A. R., *Quantum Mechanics and Path Integrals* (McGraw-Hill, New York, 1965)

confined within a hard cylinder with a radius dependent on the strength of the interaction [26], but this approximation did not fit the experimental data [27]. In Ref. [27] a more sophisticated model of a Gaussian chain confined by a harmonic potential was considered. The Gaussian chain model affords a relatively simple analytical solution, but the wormlike chain (WLC) model, based on elastic rod theory, provides a better description of the conformation of semi-flexible polyelectrolytes [28,29]. Theories of wormlike chains confined in a harmonic potential have been described in, for instance, Refs. [30,31,32,33,34]. In Ref. [33] a variational approximation was developed that combined the confined WLC model [30,32] with a more consistent description of the exponentially decaying electrostatic interaction between polyelectrolytes.

The latter polyelectrolyte theories focused primarily on the interplay between electrostatic forces and undulations at large surface separations, neglecting or not consistently incorporating shorter range image-charge forces and hard-core collisions between polyelectrolyte molecules [35]. However, because undulations bring semi-flexible polyelectrolytes into close contact, short-range forces are likely not to be negligible. Here, we demonstrate that these forces may qualitatively alter physical properties of aggregates regardless of the average surface separation.

We construct a variational theory for quasi-harmonic undulations, combining the ideas proposed in Refs. [30] and [33] with a more consistent treatment of electrostatics and hard-core collisions, at large undulation amplitudes, and a self-consistent calculation of the undulation amplitude based on the Gibbs-Bogoliubov inequality. Within this theory, we calculate pertinent pair correlation functions for the undulations and osmotic pressures of polyelectrolyte aggregates. In contrast to commonly held views, we find that undulations play a crucial role, not only in highly hydrated aggregates at large surface separations between the molecules, but also in dense columnar assemblies at surface separations comparable to, or smaller than, the Debye screening length. In the present paper we discuss the simpler case of interactions between cylindrical wormlike chains with uniform surface charge density. We will describe the more complex interplay between undulations and interactions for structured, helical polyelectrolytes in a separate study.

2. Model

Consider a columnar assembly of uniformly charged, semi-flexible polyelectrolytes that exhibit small displacements $\mathbf{r}_{j,l}(z)$ from a hexagonal lattice parallel to the z axis (Fig. 1B). The indices j and l label the molecules in the x and y directions, correspondingly (Fig. 1B). Provided that the displacement $\mathbf{r}_{j,l}(z)$ is confined within one lattice spacing (i.e., molecules do not entangle) and the tilt angle $\psi_{j,l}$ of each molecule is small ($|\psi_{j,l}|<<1$), the energy cost of the undulations may be approximated by

$$\delta E\left\{\mathbf{r}_{j,l}(z)\right\}=\delta E_b\left\{\mathbf{r}_{j,l}(z)\right\}+\delta E_{el}\left\{\mathbf{r}_{j,l}(z)\right\}+\delta E_{st}\left\{\mathbf{r}_{j,l}(z)\right\}, \quad (1)$$

where $\delta E_b\{\mathbf{r}_{j,l}(z)\}$, $\delta E_{el}\{\mathbf{r}_{j,l}(z)\}$, and $\delta E_{st}\{\mathbf{r}_{j,l}(z)\}$ are the energetic costs of bending, the energy of electrostatic interactions between molecules, and the energy attributable to steric (hard-core) collisions between the molecules, respectively. For the purpose of the present study, we neglect entanglement and sharp bending of the molecules, which may introduce additional corrections to the free energy of polyelectrolyte aggregates [36].

We describe the cost of bending within the wormlike chain approximation [28,29] as

$$\delta E_b\left\{\mathbf{r}_{j,l}(z)\right\}=\sum_{j,l}\int_0^L dz\frac{l_p^b}{2}\left(\frac{d^2\mathbf{r}_{j,l}(z)}{dz^2}\right)^2, \tag{2}$$

where L is the total length and l_p^b is the persistence length of the molecules.

2.1 Electrostatic energy

We calculate the electrostatic cost of undulations by pairwise summation of interactions of each molecule with its six nearest neighbors [21],

$$\delta E_{el}\left\{\mathbf{r}_{j,l}(z)\right\}=\frac{1}{2}\sum_{j,l}\sum_{i=1}^{6}\int_0^L dz\left[u_{cyl}\left(R_0,\delta r_{j,l}(z)\right)-u_{cyl}(R_0,0)\right], \tag{3}$$

where [37]

$$u_{cyl}(R_0,\delta r)\approx\frac{2\xi_{eff}^2}{l_B}\left\{K_0\left[\kappa(R_0+\delta r)\right]-\sum_{j=-\infty}^{\infty}\left(K_j\left[\kappa(R_0+\delta r)\right]\right)^2\frac{I_j'(\kappa a)}{K_j'(\kappa a)}\right\}; \tag{4}$$

$$\xi_{eff}=\frac{l_B}{\tilde{l}_c\cdot\kappa a\cdot K_1(\kappa a)}; \tag{5}$$

ξ_{eff} is a dimensionless effective Manning parameter that can be calculated, e.g., as described in Ref. [38]; l_B is the Bjerrum length (7 Å in water); $\tilde{l}_c$ is the effective distance per unit charge along the molecules, which accounts for partial charge neutralization by bound/condensed counterions (e.g., within the Manning model $\tilde{l}_c=l_B$, when the distance per unit fixed/bare charge l_c is less than l_B); a is the molecule radius (we assume that water-impenetrable core of the molecule has a low dielectric constant); κ is the inverse screening length in the assembly; $I_n(x)$, $K_n(x)$, $I'_n(x)$, and $K'_n(x)$ are the modified Bessel functions and their derivatives, respectively; the index i labels the six nearest neighbors of each molecule (j,l); and $\delta r_{j,l,i}(z)$ is the change in the interaxial distance between the molecule (j,l) and its neighbors due to undulations. The second term in Eq. (4) describes the contribution of image-charge forces associated with dielectric cores of the molecules. For simplicity, hereafter all energies and free energies are dimensionless, measured in the units of the thermal energy k_BT.

Note that κ is generally larger than the inverse Debye screening length κ_D in the surrounding electrolyte solution outside the aggregate, because of the accumulation of additional counterions within the assembly [21]. The relationship between κ and κ_D can be approximated within the cylindrical cell model, in which the hexagonal Wigner-Seitz cell of each molecule is replaced with a cylinder of the same volume. In this model [39]

$$\kappa=\kappa_D\sqrt{\cosh(e\varphi_s/k_BT)}, \tag{6}$$

$$\tanh\left(\frac{e\varphi_s}{k_BT}\right)=2\xi_{eff}\frac{[I_0(\kappa R_s)K_1(\kappa R_s)+I_1(\kappa R_s)K_0(\kappa R_s)]}{\left[I_1(\kappa R_s)-K_1(\kappa R_s)\frac{I_1(\kappa a)}{K_1(\kappa a)}\right]}, \tag{7}$$

where φ_s is the electrostatic potential at the surface of the effective cylindrical Wigner-Seitz cell and

$$R_s=R_0\sqrt{\sqrt{3}/2\pi}. \tag{8}$$

is the radius of this cell. Note that the present, simplified form of Eqs. (6)–(8) is appropriate only for 1:1 electrolyte solutions; more general expressions can be found in Ref. [39].

2.2 Steric confinement (Helfrich-Harbich model)

To model steric confinement, we utilize the approximation proposed by Helfrich and Harbich [30,26]. Specifically, we replace $\delta E_{st}\{\mathbf{r}_{j,l}(z)\}$ with an effective Gaussian confinement potential

$$\delta E_{st}^{eff}\{\mathbf{r}(z)\}=\frac{\alpha_0}{2}\int_0^L dz\left[\mathbf{r}(z)^2\right], \tag{9}$$

in which the parameter α_0 is selected to provide the same mean square displacement of uncharged molecules. Since the maximum displacement is ~ R_0-2a, we may expect [30]

$$\left\langle\mathbf{r}(z)^2\right\rangle=\mu(R_0-2a)^2. \tag{10}$$

Here $\mu<1$ is a dimensionless constant, e.g., simulations for a confined wormlike chain suggest that $\mu\approx 1/2$ [40].

Calculation of $\langle\mathbf{r}(z)^2\rangle$ with the energy functional given by Eq. (9) and a comparison with Eq. (10) then yields

$$\alpha_0=\frac{1}{2^{2/3}\mu^{4/3}(R_0-2a)^{8/3}\left(l_p^b\right)^{1/3}}. \tag{11}$$

2.3 Variational approximation

To calculate the free energy and correlation functions for the undulations, we utilize a variational approximation, in which we replace $\delta E\{\mathbf{r}_{j,l}(z)\}$ with an effective energy,

$$\delta E_{eff}\left\{\mathbf{r}_{j,l}(z)\right\}=\frac{1}{2}\sum_{j,l}\int_0^L dz\left[l_p^b\left(\frac{d^2\mathbf{r}_{j,l}(z)}{dz^2}\right)^2+\alpha\mathbf{r}_{j,l}(z)^2\right], \tag{12}$$

where α is a variational parameter. We then define the following free energy functional

$$F_{und}\approx-\ln\delta Z_{eff}+\left\langle\delta E\left\{\mathbf{r}_{j,l}(z)\right\}-\delta E_{eff}\left\{\mathbf{r}_{j,l}(z)\right\}\right\rangle_{eff}, \tag{13}$$

where

$$\delta Z_{eff} = \prod_{j,l} \int D\mathbf{r}_{j,l}(z) \exp\left[-\delta E_{eff}\left\{\mathbf{r}_{j,l}(z)\right\}\right] \tag{14}$$

is the partition function for the effective energy; and $< >_{eff}$ indicates averaging with the statistical weight of exp [$-\delta E_{eff}\{\mathbf{r}_{j,l}(z)\}$], i.e.,

$$\left\langle f\left\{\mathbf{r}_{j,l}(z)\right\}\right\rangle_{eff} \equiv \frac{1}{\delta Z_{eff}} \prod_{j,l} \int D\mathbf{r}_{j,l}(z)\, f\left\{\mathbf{r}_{j,l}(z)\right\} \exp\left[-\delta E_{eff}\left\{\mathbf{r}_{j,l}(z)\right\}\right] \tag{15}$$

for any functional $f\mathbf{r}_{j,l}(z)$. Here, $\int D\mathbf{r}_{j,l}(z)$ corresponds to path integration [41] over both components of the displacement vector $\mathbf{r}_{j,l}(z)$.

The Gibbs-Bogoliubov inequality [42] states that the right hand side of Eq. (13) is always larger or equal to the exact free energy at any α. Therefore, we approximate the undulation free energy by the value of F_{und} minimized with respect to α.

As any model with unlimited fluctuations, this approximation effectively allows the cores of the molecules to overlap (e.g., at $\delta r_{j,l,i}(z) < 2a - R_0$). Within this unphysical overlap region, $\delta E_{el}\{\mathbf{r}_{j,l}(z)\}$ is not defined; it has to be put into the model artificially. In previously used models [33,34,25], the expression for $\delta E_{el}\{\mathbf{r}_{j,l}(z)\}$ derived outside of the overlap was simply extended into the overlap region. As long as the contribution of this region to the free energy and relevant correlation functions is small, the unphysical overlap does not present a problem. However, this may not always be the case.

To avoid the latter problem, we define $\delta E_{el}\{\mathbf{r}_{j,l}(z)\}$ in such a way that it does not generate any artificial forces within the unphysical overlap region or at the boundary of this region. Specifically, $\delta E_{el}\{\mathbf{r}_{j,l}(z)\}$ remains constant throughout this region and equal to its value at the region boundary, i.e., we replace Eq. (3) with

$$\delta E_{el}\left\{\mathbf{r}_{j,l}(z)\right\} \approx \frac{1}{2}\sum_{j,l}\sum_{i=1}^{6}\int_0^L dz\left[\delta u_{j,l,i}(R_0, z)\right], \tag{16}$$

where

$$\delta u_{j,l,i}(R_0, z) = \begin{cases} u_{cyl}\left(R_0, \delta r_{j,l,i}(z)\right) - u_{cyl}(R_0, 0), & |\delta r_{j,l,i}(z)| \le R_0 - 2a \\ u_{cyl}(R_0, R_0 - 2a) - u_{cyl}(R_0, 0), & \delta r_{j,l,i}(z) > R_0 - 2a \\ u_{cyl}(R_0, 2a - R_0) - u_{cyl}(R_0, 0), & \delta r_{j,l,i}(z) < 2a - R_0 \end{cases} . \tag{17}$$

In addition, provided that $2\kappa a >> 1$ and $\delta r/R_0 << 1$, we may approximate Eq. (4) with

$$u_{cyl}(R_0, \delta r) \approx \frac{\xi_{eff}^2 \sqrt{2\pi} \exp\left[-\kappa(R_0 + \delta r)\right]}{l_B (\kappa R_0)^{1/2}} + \frac{\xi_{eff}^2 \pi \Omega_0 \exp\left[-2\kappa(R_0 + \delta r)\right]}{l_B (\kappa R_0)} \tag{18}$$

where

$$\Omega_0 = -\Sigma_j I_j'(\kappa a)/K_j'(\kappa a). \tag{19}$$

Equations (12)–(14) combined with (1), (2), (9), (11), (16) and (17) fully define the model we use for calculating all relevant correlation functions and the contribution of undulations to the aggregate free energy.

2.4 Osmotic pressure

The effective osmotic pressure of the aggregate is given by

$$\Pi = \Pi_0 + \Pi_{und}, \tag{20}$$

where

$$\Pi_0 = \frac{\kappa_D^2 k_B T}{4\pi l_B}\left[\cosh\left(\frac{e\varphi_s}{k_B T}\right) - 1\right] \tag{21}$$

is the osmotic pressure of an aggregate of straight molecules [43], and

$$\Pi_{und} = -k_B T\left(\frac{\partial F_{und}}{\partial V_w}\right)_\kappa = -\frac{k_B T}{NLR_0\sqrt{3}}\left(\frac{\partial F_{und}}{\partial R_0}\right)_\kappa \tag{22}$$

is the contribution from undulations. In Eq. (22), the k_BT prefactor provides dimensionality to the dimensionless undulation free energy F_{und}, and F_{und} is calculated from Eq. (13) and by minimization with respect to α. The partial derivative of F_{und} is taken at fixed κ to account for the averaging over the counter-ion degrees of freedom.

3. Results

3.1 Pair correlation functions

Within our model, the pair correlation function for undulations is given by (see Appendix)

$$\left\langle \mathbf{r}_{j,l}(z)\,\mathbf{r}_{m,n}(z')\right\rangle = \delta_{j,m}\delta_{l,n}G(z-z'), \tag{23}$$

where

$$G(z-z') = d^2\sqrt{2}\cos\left(\frac{|z-z'|}{\sqrt{2}\lambda_B} - \frac{\pi}{4}\right)\exp\left(-\frac{|z-z'|}{\sqrt{2}\lambda_B}\right), \tag{24}$$

$$d = \left(4\alpha^3 l_p^b\right)^{-1/8} \tag{25}$$

is the rms undulation amplitude, and

$$\lambda_B = \left(\sqrt{2} d^2 l_p^b\right)^{1/3} \tag{26}$$

is the undulation correlation length (first introduced by Odijk [44,45]).

Note that our approximation for the electrostatic energy is valid only at small fluctuations of the tilt angle ψ of each molecule with respect to the vertical position (Fig. 1A). The mean square amplitude of the latter fluctuations is given by (Appendix)

$$\langle \psi \rangle^2 = \frac{1}{2} \left\langle \left(\frac{d\mathbf{r}(z)}{dz} \right)^2 \right\rangle = \left(\frac{d}{4 l_p^b} \right)^{2/3}, \tag{27}$$

indicating that the present theory is valid at

$$\left(\frac{d}{4 l_p^b} \right)^{1/3} \ll 1. \tag{28}$$

It may be possible to account for undulations with larger tilt angles utilizing the ideas developed in Ref. [46], but such a theory would be substantially more complicated.

3.2 Free energy and amplitude of undulations

As shown in the Appendix, the calculation of F_{undl} from Eqs. (1)–(3), (9), (11), (12)–(18), and (25) yields

$$\begin{aligned} \frac{F_{und}}{NL} \approx & \frac{1}{2^{5/3} d^{2/3} (l_p^b)^{1/3}} \left[3 + \frac{d^{8/3}}{\mu^{4/3} (R_0 - 2a)^{8/3}} \right] \\ & + \frac{3 \xi_{eff}^2 \sqrt{2\pi} \exp(-\kappa R_0)}{l_B (\kappa R_0)^{1/2}} \gamma\left(\kappa (R_0 - 2a), \kappa d\right), \\ & + \frac{3 \xi_{eff}^2 \pi \Omega_0 \exp(-2\kappa R_0)}{l_B (\kappa R_0)} \gamma\left(2\kappa (R_0 - 2a), 2\kappa d\right) \end{aligned} \tag{29}$$

where

$$\begin{aligned} \gamma(x, y) = & -1 + \cosh(x) \left[1 - \operatorname{erf}\left(\frac{x}{y\sqrt{2}} \right) \right] \\ & + \frac{1}{2} e^{\frac{y^2}{2}} \left[\operatorname{erf}\left(\frac{x}{y\sqrt{2}} - \frac{y}{\sqrt{2}} \right) + \operatorname{erf}\left(\frac{x}{y\sqrt{2}} + \frac{y}{\sqrt{2}} \right) \right]. \end{aligned} \tag{30}$$

We expressed F_{und} as a function of the rms undulation amplitude d rather than as a function of the variational parameter α, by utilizing Eq. (25), thus establishing a relationship between d and α. Minimization of F_{und} with respect to α is equivalent to minimization with respect to d. From this minimization we find

$$\frac{l_B}{2^{2/3}\kappa^2 d^{8/3}\left(l_p^b\right)^{1/3}}\left[1-\frac{d^{8/3}}{\mu^{4/3}(R_0-2a)^{8/3}}\right]= \frac{3\sqrt{2\pi}\xi_{eff}^2\exp(-\kappa R_0)}{(\kappa R_0)^{1/2}}\eta\left(\kappa\left(R_0-2a\right),\kappa d\right), +\frac{12\pi\xi_{eff}^2\Omega_0\exp(-2\kappa R_0)}{(\kappa R_0)}\eta\left(2\kappa\left(R_0-2a\right),2\kappa d\right) \tag{31}$$

where

$$\eta(x,y) = \frac{1}{2}e^{\frac{y^2}{2}}\left[\operatorname{erf}\left(\frac{1}{\sqrt{2}}\left(\frac{x}{y}+y\right)\right)+\operatorname{erf}\left(\frac{1}{\sqrt{2}}\left(\frac{x}{y}-y\right)\right)\right] -\frac{2}{y\sqrt{2\pi}}\sinh(x)\exp\left(-\frac{x^2}{2y^2}\right). \tag{32}$$

One may now calculate the undulation amplitude by solving Eqs. (31) and (32) with respect to *d*. For uncharged molecules (ξ_{eff}=0), we recover $d^2 \equiv \left\langle \mathbf{r}_{j,l}^2 \right\rangle = \mu(R_0 - 2a)^2$ (c.f., Eq. (10)). Because η(*x*,*y*) is positively defined, electrostatic repulsion between charged molecules reduces the undulation amplitude as one might expect.

Figure 2 illustrates the dependence of the undulation amplitude *d* on the average surface-to-surface separation between the molecules (R_0−2*a*) at different linear charge densities $\xi = l_B/\tilde{l}_c$ (Fig. 2A) and different bending persistence lengths l_p^b (Fig. 2B). The results are represented in dimensionless form, in which they are nearly independent of the specific values of κ_D and *a*.

As follows from Eq. (31), *d* depends explicitly on ξ and l_p^b through a single parameter, $\xi^2\left(l_p^b\right)^{1/3}$. Although *d* also depends implicitly on ξ through κ (Fig. 2A, inset), the latter effect is weak for moderately charged molecules (ξ < 2), as shown by the dotted-line curve in Fig. 2A. For such molecules, increasing the charge density (Fig. 2A) and increasing the persistence length (Fig. 2B) have similar effects on the undulation amplitude.

3.3 Highly charged polyelectrolytes

Formally, Eqs. (29)–(32) can be simplified for highly charged molecules in the case of strong electrostatic confinement $\left(d^2 << \mu(R_0 - 2a)^2, \kappa d^2 << R_0 - 2a\right)$ and negligible image-charge forces. In this case, $\gamma(x,y) \approx \eta(x,y) \approx e^{y^2/2}$ and

$$\frac{\kappa l_B}{3\sqrt{2\pi}\xi_{eff}^2\left(4\kappa l_p^b\right)^{1/3}} \approx (\kappa d)^{8/3}\frac{\exp\left(-\kappa R_0+\kappa^2 d^2/2\right)}{(\kappa R_0)^{1/2}}. \tag{33}$$

This equation is similar to the one reported in [33], except the left hand side in our case is larger by a factor of 3/2 and we do not assume $\kappa \approx \kappa_D$. The numerical discrepancy appears to be related to the difference between the *ad hoc* approximation for the free energy in Ref. [33] and the more rigorous approximation based on the Gibbs-Bogoliubov inequality utilized in the present work.

Eq. (33) works reasonably well at ξ >> 1 (Fig. 2B). At ξ ~ 1, Eq. (33) fails in two ways: (i) At surface separations up to ~ $1/\kappa_D$, the undulation amplitude is determined primarily by steric confinement even for very rigid polyelectrolytes. At these distances, Eq. (33) predicts

unphysically large d, exceeding the undulation amplitude for uncharged molecules (which is restricted by steric collisions). As a result, it predicts a large unphysical enhancement of the mean electrostatic force. (ii) At large separations, Eq. (33) strongly underestimates d for flexible polyelectrolytes; it does not consistently account for the steric confinement, extending the exponential electrostatic interaction into the region where the molecules overlap (see also the discussion of Eqs. (16) and (17)). Numerical comparison of Eqs. (31) and (32) with Eq. (33) suggests that neither steric confinement nor image forces can be neglected for flexible polyelectrolytes with $\xi \sim 1$ at any separation.

3.4 Osmotic pressure

The aggregate osmotic pressure is given by Eqs. (20)–(22). After substitution of Eqs. (29) and (30) into Eq. (22) we find that the contribution of undulations to the osmotic pressure is described by

$$\Pi_{und}=\Pi_{und}^{st}+\Pi_{und}^{el}, \tag{34}$$

where

$$\Pi_{und}^{st} \approx \frac{2^{4/3}}{3\sqrt{3}} k_B T \frac{d^2}{\mu^{4/3}\left(l_p^b\right)^{1/3} R_0 (R_0-2a)^{11/3}} \tag{35}$$

results from the steric collisions between the molecules and

$$\Pi_{und}^{els} \approx \sqrt{3} k_B T \frac{\kappa \xi_{eff}^2}{R_0 l_B}\left[\frac{\sqrt{2\pi}\exp(-\kappa R_0)}{(\kappa R_0)^{1/2}}\chi\left(\kappa(R_0-2a),\kappa d\right)+\frac{2\pi\Omega_0\exp(-2\kappa R)}{(\kappa R_0)}\chi\left(2\kappa(R_0-2a),2\kappa d\right)\right], \tag{36}$$

with

$$\chi(x,y)=-1+e^{-x}\left[1-\operatorname{erf}\left(\frac{x}{y\sqrt{2}}\right)\right]+\frac{1}{2}e^{\frac{y^2}{2}}\left[\operatorname{erf}\left(\frac{x}{y\sqrt{2}}-\frac{y}{\sqrt{2}}\right)+\operatorname{erf}\left(\frac{x}{y\sqrt{2}}+\frac{y}{\sqrt{2}}\right)\right], \tag{37}$$

is the electrostatic component of the undulation osmotic pressure.

As illustrated in Fig. 3, undulations provide the dominant contribution to the osmotic pressure at small and large separations, regardless of polyelectrolyte charge and rigidity. At small separations, via steric collisions, the entropic cost associated with the elimination of undulations diverges as the separation between molecules approaches zero, while the electrostatic interaction energy remains finite. At large separations, undulations extend and enhance the short-range electrostatic repulsion by bringing parts of the molecules much closer together. Although, in this case, $\prod_{und}^{st}$ is small compared with $\prod_{und}^{els}$, steric collisions still play an important role in limiting electrostatic interactions, reducing the undulation amplitude and limiting the enhancement of the electrostatic interaction (through the erf-functions in Eq. (37)).

4. Discussion

The present study suggests that undulations significantly contribute to interactions between polyelectrolytes at all surface separations, even in well-ordered columnar aggregates (Fig. 3).

The undulations become negligible only for rigid, highly charged ($\xi >>1$) polyelectrolytes and even then only at surface separations close to $1/\kappa_D$, which are not common conditions since counterion condensation and binding reduce ξ in polyelectrolytes with a high density of fixed surface charges. Indeed, $\xi \leq 1$ for all polyelectrolytes in the limit of infinitely dilute salt [47]. Large ξ is possible only at finite salt concentrations in the absence of counterions that may strongly bind to the polyelectrolyte [48].

The effect of enhancement of electrostatic interactions by undulations at large separations was well recognized before us [27,33,25]. However, the contribution from undulations at intermediate and small separations was not. We now find that, depending on the polyelectrolyte charge and rigidity, undulations may significantly shift the whole osmotic pressure curve. Figs. 3A and 3B illustrate this effect for uniformly charged worm-like chains with DNA-like diameter and rigidity at physiological ionic strength. The value of $\xi = 0.5$ corresponds to 87% neutralization of DNA charge by counterions, a value that models the binding (or condensation) of Ca^{2+}, Mg^{2+} and other divalent and polyvalent counterions under physiological conditions; $\xi = 2$ corresponds to 50% neutralization of DNA charge, which approximates counterion condensation in monovalent salt solutions at physiological ionic strength [21,48,49].

These findings are in sharp contrast with the commonly held view [27] that undulations are important only in hydrated aggregates at large separations. Our model differs from previous theories in several aspects, e.g., it accounts for image-charge forces due to water-impermeable cores of polyelectrolyte molecules. However, its most important distinction, primarily responsible for the discrepancy, is a more consistent treatment of steric collisions between the molecules. Previous theories [27,33,34,25] effectively presumed a purely electrostatic suppression of otherwise unlimited undulations, resulting in an infinite undulation amplitude for uncharged molecules and a finite, nonzero undulation amplitude at zero surface separation between charged molecules. Our model accounts for steric confinement of undulations by hard-core collisions, introducing the corresponding steric confinement energy based on the idea proposed by Helfrich and Harbich for uncharged worm-like chains [30]. Like the previous theories, our model is based on a quasi-Gaussian description of undulations, but it captures the limiting cases of uncharged molecules and small surface separations (Fig. 2).

In our calculations, we have assumed local hexagonal packing of the molecules in a columnar assembly. We should bear in mind, however, that undulations may induce a melting (deconfinement) phase transition at $d = cR_0$ (the Lindeman criterion), where the constant c has been estimated to be $c \sim 0.15 – 0.48$ [50,34,25]. A theory for this transition was proposed in Ref. [24]. It included an estimate of steric interactions, but it was based on an oversimplified description of the hexagonal phase and electrostatic interactions. Perhaps, our work in conjunction with Ref. [24] may form the basis of a more accurate theory [51].

We believe that the present study makes an important step towards a better understanding of the physics of interactions between uniformly charged worm-like chains in a continuum electrolyte solution with point-like, weakly coupled salt ions. At the same time, it is worthwhile to keep in mind the limitations of such a description for real polyelectrolytes. This description is likely to be reasonable, at least qualitatively, when the distance scales for neglected effects (e.g., ion size) are smaller than the pertinent characteristic lengths in the theory, e.g., the effective screening length and surface-surface separation [52].

Eqs. (34)–(37) provide a recipe for understanding the physics of osmotic pressures in polyelectrolyte aggregates. The osmotic pressure is not just a commonly used method for studying such aggregates (see, e.g., [21,53,54] and refs. therein) but also a functionally important property of cartilage and other natural and engineered systems [55,56,57]. Eqs. (34)–(37) predict osmotic pressures (Fig. 3) that are qualitatively and semi-quantitatively consistent

with the measurements [58,59], but we urge caution in more detailed quantitative comparisons with experiments. Eqs. (34)–(37) have not been designed for and may not be sufficiently accurate for analysis of specific experimental data. For the latter purpose, the approximations of uniform surface charge density and hexagonal packing may not be appropriate; and these equations may have to be modified to account for specific details of the system under study.

One factor that has to be taken into account for practical applications is the polyelectrolyte structure, particularly when the distance between regularly organized surface charges exceeds the effective screening length inside aggregates (3–10 Å in typical experiments). In the latter case, the uniform surface charge approximation may, e.g., severely underestimate image-charge forces and completely miss crucially important effects associated with mutual alignment of the molecules [21]. We will illustrate these effects and ways to modify the model to account for them in a separate study of DNA, for which the surface charge periodicity defined by the 34 Å helical pitch is much larger than the screening length, resulting in rather nontrivial effects of undulations on helix-specific interactions.

Similarly, the extent and patterns of counterion binding/condensation may need to be treated at a more sophisticated level than simply by employing an effective Manning parameter, e.g., long-range correlations between multi- and polyvalent ions at the polyelectrolyte surface may need to be explicitly incorporated into the theory, when such counterions are present in the solution [60]. Work in this direction is currently in progress.

5. Conclusions

1. In contrast to previous models, the present theory describes the intermolecular interactions within an assembly of undulating, semi-flexible polyelectrolytes for both the limiting cases of uncharged and highly-charged molecules as well as for polyelectrolytes with more practically important, intermediate linear charge densities.

2. In the limit of small surface separations, hard-core collisions provide the dominant interaction between undulating, uniformly-charged, semi-flexible polyelectrolytes confined in a columnar aggregate, regardless of the polyelectrolyte charge density.

3. At effective linear charge densities comparable to or smaller than one elementary charge per Bjerrum length, the steric confinement due to hard-core collisions significantly affects aggregate osmotic pressures at all interaxial separations.

Acknowledgments

This work was supported in part by the Max-Planck Society (Lee), the Intramural Research Program of NICHD, NIH (Leikin), and the Alexander von Humboldt Foundation (Wynveen).

Appendix

Correlation functions

After representing $\mathbf{r}_{j,l}(z)$ by Fourier series,

$$\mathbf{r}_{j,l}(z) = \sum_k \tilde{\mathbf{r}}_{j,l} e^{ikz}, \tag{A.1}$$

the expression for the effective free energy (Eq. (12)) can be rewritten as

$$\delta E_{eff}\left\{\mathbf{r}_{j,l}(k)\right\}=\frac{L}{2}\sum_{j,l}\sum_{k}\left(l_p^b k^4+\alpha\right)\tilde{\mathbf{r}}_{j,l}(k)\,\tilde{\mathbf{r}}_{j,l}(-k)\,. \tag{A.2}$$

Applying the equipartition theorem [1],

$$\left\langle\tilde{\mathbf{r}}_{j,l}(k)\,\tilde{\mathbf{r}}_{n,m}(-k)\right\rangle=\frac{2\delta_{j,n}\delta_{l,m}}{L\left(l_p^b k^4+\alpha\right)}, \tag{A.3}$$

we then find

$$\left\langle\left(\mathbf{r}_{j,l}(z)-\mathbf{r}_{j,l}(z')\right)^2\right\rangle=2G(0)-2G(z-z')\,, \tag{A.4}$$

where (in the limit of $L\to\infty$)

$$G(z-z')=\frac{1}{\pi}\int_{-\infty}^{\infty}dk\frac{\exp\left(ik\left(z-z'\right)\right)}{l_p^b k^4+\alpha}. \tag{A.5}$$

Contour integration of Eq. (A.5) in the top half on the complex plane yields

$$G(z-z')=\frac{(\lambda_B)^3}{l_p^b}\exp\left(-\frac{|z-z'|}{\sqrt{2}\lambda_B}\right)\cos\left(\frac{|z-z'|}{\sqrt{2}\lambda_B}-\frac{\pi}{4}\right), \tag{A.6}$$

with the correlation length for bending fluctuations,

$$\lambda_B=\left(\frac{l_p^b}{\alpha}\right)^{1/4}. \tag{A.7}$$

Since $G(z-z')$ exponentially decreases at $|Z-Z'|\gg\lambda_B$, the centerline of each rod is effectively confined within a cylinder with the radius

$$d=\sqrt{G(0)}. \tag{A.8}$$

From Eqs. (A.6)–(A.8) we recover Eqs. (25) (26) of the main text. Note that this approximation may also be used at finite L provided that $L>>\lambda_B$.

From similar calculations we find another useful correlation function

$$\left\langle\frac{d\mathbf{r}_{j,l}(z)}{dz}\bullet\frac{d\mathbf{r}_{j,l}(z')}{dz'}\right\rangle=\frac{\lambda_B}{l_p^b}\exp\left(-\frac{|z-z'|}{\sqrt{2}\lambda_B}\right)\cos\left(\frac{|z-z'|}{\sqrt{2}\lambda_B}+\frac{\pi}{4}\right), \tag{A.9}$$

The special case of this correlation function at $z=z'$ defines the mean square fluctuations of the tilt angle ψ given by Eq. (27) of the main text.

Variational free energy

To calculate $\ln(\delta Z_{eff})$, we use that

$$-\frac{1}{NL}\frac{\partial}{\partial\alpha}\ln\left(\delta Z_{eff}\right)=\frac{\left\langle \mathbf{r}^2\right\rangle_{eff}}{2}=\frac{d^2}{2}. \tag{A.10}$$

After integration, we find

$$-\frac{1}{NL}\ln\left(\delta Z_{eff}\right)=\left(\frac{2}{d^2 l_p^b}\right)^{1/3}, \tag{A.11}$$

where the integration constant was selected from the assumption that $F_{und}=0$ at $F_{und}=0 \quad \text{at} \quad l_p^b \to \infty$.

To calculate $\left\langle \delta E\left\{\mathbf{r}_{j,l}(z)\right\}-\delta E_{eff}\left\{\mathbf{r}_{j,l}(z)\right\}\right\rangle_{eff}$, we utilize that for any ergodic random process $\mathbf{r}_{j,l}(z)$ [2],

$$\left\langle f\left\{\mathbf{r}_{j,l}(z)\right\}\right\rangle_{eff}\equiv\left\langle\int\tilde{f}\left(\mathbf{r}_{j,l}(z)\right)dz\right\rangle_{eff}=L\left\langle\tilde{f}\left(\mathbf{r}_{j,l}(z)\right)\right\rangle_{eff}=L\int\tilde{f}(\mathbf{r})\,P(\mathbf{r})\,d\mathbf{r} \tag{A.12}$$

whrere $\tilde{f}(\mathbf{r})$is an arbitrary function of $\mathbf{r}$. The probability density $P(\mathbf{r})$ for a Gaussian random process is given by [2]

$$P(\mathbf{r})=\frac{1}{4\pi^2}\int d\mathbf{u}e^{-i\mathbf{ur}}\left\langle e^{i\mathbf{ur}'(z)}\right\rangle_{eff}=\frac{1}{\pi}e^{\frac{\mathbf{r}^2}{\langle\mathbf{r}^2\rangle}}=\frac{1}{\pi}e^{\frac{\mathbf{r}^2}{d^2}}, \tag{A.13}$$

where we took into account that $\mathbf{r}(z)$ is a 2D vector. From Eqs.(2) (9) (12) (13) (16), we find

$$\frac{1}{NL}\left\langle \delta E\left\{\mathbf{r}_{j,l}(z)\right\}-\delta E_{eff}\left\{\mathbf{r}_{j,l}(z)\right\}\right\rangle_{eff}=\frac{\alpha_0-\alpha}{2}d^2+3\left\langle\delta u_{j,l,i}(R_0,z)\right\rangle_{eff}, \tag{A.14}$$

where $\delta u_{j,l,i}(R_0, z)$ is given by Eq. (17) of the main text.

Since $\left\langle\delta u_{j,l,i}(R_0,z)\right\rangle_{eff}$ does not depend on j, l, or i, it is to calculate $\left\langle\delta u_{j,l,3}(R_0,z)\right\rangle_{eff}$ (see Fig. 1b). At small $x_{j,l}$ and $y_{j,l}$ displacements of the molecules (j,l) and $(j+1,l)$, i.e., $|x_{j+1,l}-x_{j,l}|/R_0 << 1$ and $|y_{j+1,l}-y_{j,l}|/R_0 << 1$,

$$\delta r_{j,l,3}(z)\approx\left(x_{j+1,l}-x_{j,l}\right), \tag{A.15}$$

where we neglected the second order terms with respect to $x_{j+1,l}-x_{j,l}$ and $y_{j+1,l}-y_{j,l}$. After substituting Eqs. (17), (A.14), (A.15) into Eqs. (A.12), (A.13), we then find

$$\left\langle \delta u_{j,l,3}(R_0,z)\right\rangle_{eff} \approx \frac{1}{d\sqrt{2\pi}} \times\left[u_{cyl}(R_0,2a-R_0)\int_{-\infty}^{2a-R_0}\exp\left(-\frac{\delta x^2}{2d^2}\right)d(\delta x) +\int_{2a-R_0}^{R_0-2a}u_{cyl}(R_0,\delta x)\exp\left(-\frac{\delta x^2}{2d^2}\right)d(\delta x) u_{cyl}(R_0,R_0-2a)\int_{R_0-2a}^{\infty}\exp\left(-\frac{\delta x^2}{2d^2}\right)d(\delta x)\right], \quad (A.16)$$

where we changed the integration variables from $x_{j+1,l}$ and $x_{j,l}$ to $\delta x = x_{j+1,l} - x_{j,l}$ and $x_{j+1,l} + x_{j,l}$ and integrated out $x_{j+1,l} + x_{j,l}$.

At $\kappa a >> 1$, substitution of Eq. (18) into Eq. (A.16) yields

$$\left\langle \delta u_{j,l,3}(R_0,z)\right\rangle_{eff} \approx \frac{\xi_{eff}^2\sqrt{2\pi}\exp(-\kappa R_0)}{l_B(\kappa R_0)^{1/2}}g(\kappa(R_0-2a),\kappa d)+\frac{\xi_{eff}^2\pi\Omega_0\exp(-2\kappa R_0)}{l_B(\kappa R_0)}g(2\kappa(R_0-2a),2\kappa d) \quad (A.17)$$

where $g(x,y)$ is defined by Eq. (30). Finally, after substituting Eqs. (A.11), (A.14), and (A.17) into Eq. (13), we arrive at Eq. (29) of the main text.

References

1. Knaapila M, Almasy L, Garamus VM, Pearson C, Pradhan S, Petty MC, Scherf U, Burrows HD, Monkman AP. J. Phys. Chem. B 2006;110:10248. and references contained therin. [PubMed: 16722726]
2. Guilleaume B, Blaul J, Wittemann M, Rehahn M, Ballauff M. J. Phys: Condens. Matter 2000;12:A245.
3. Zaroslov YD, Gordeliy VI, Kuklin AI, Islamov AH, Philippova OE, Khokhlov AR, Wegner G. Macromolecules 2002;35:4466.
4. Tang JX, Ito T, Tao T, Traub P, Janmey PA. Biochemisty 1997;36:12600.
5. Livolant F, Bouligand Y. J. Phys. France 1986;47:1813.
6. Podgornik R, Rau DC, Parsegian VA. Macromolecules 1989;22:1780.
7. Rau DC, Lee B, Parsegian VA. Proc. Natl. Acad. Sci. USA 1984;81:2621. [PubMed: 6585818]
8. Tang JX, Janmey PA. J. Bio. Chem 1996;271:8556. [PubMed: 8621482]
9. Kwon HJ, Kakugo A, Shikinaka K, Osada Y, Gong JP. Biomacromolecules 2005;6:3005. [PubMed: 16283720]
10. Angelini TE, Liang H, Wriggers W, Wong GCL. Proc. Natl. Acad. Sci. USA 2003;100:8634. [PubMed: 12853566]
11. Angelini TE, Liang H, Wriggers W, Wong GCL. Eur. Phys. J 2005;16:389.
12. Rau DC, Parsegian VA. Science 1990;249:1278. [PubMed: 2144663]
13. Nedoluzhko A, Douglas T. J. Inorg. Biochem 2001;84:233. [PubMed: 11374586]
14. Parsegian VA, Brenner SL. Nature 1976;259:632. [PubMed: 1250412]
15. Klimenko SM, Tikchonenko TI, Andreev VM. J. Mol. Biol 1967;23:523. [PubMed: 6032188]
16. Earnshaw WC, Harrison SC. Nature 1977;268:598. [PubMed: 401433]
17. Tzlil S, Kindt JT, Gelbart WM, Ben-Shaul A. Biophys. J 2003;84:1616. [PubMed: 12609865]
18. Glenny JR, Kaulfus P, Matsudaira P, Weber K. J. Bio. Chem 1981;256:9283. [PubMed: 6894925]
19. Widom J, Baldwin RL. J. Mol. Biol 1980;144:431. [PubMed: 6454789]
20. Todd BA, Parsegian VA, Shirahata A, Thomas TJ, Rau DC. Biophys. J 2008;94:4775. [PubMed: 18326632]
21. Kornyshev AA, Lee DJ, Leikin S, Wynveen A. Rev. Mod. Phys 2007;79:943.
22. Bloomfield VA. Curr. Opin. Struct. Biol 1996;6:334. [PubMed: 8804837]
23. Selinger JV, Bruinsma RF. Phys. Rev. A 1991;43:2910. [PubMed: 9905358]

24. Selinger JV, Bruinsma RF. Phys. Rev. A 1991;43:2922. [PubMed: 9905359]
25. Strey HH, Parsegian VA, Podgornik R. Phys. Rev. E 1999;59:999.
26. Stigter D. Cell Biochem. Biophys 1987;11:139.
27. Podgornik R, Parsegian VA. Macromolecules 1990;23:2265.
28. Kratky O, Porod G. Rec. Trav. Chim. Pays-Bas 1949;68:1106.
29. Fixman M, Kovac J. J. Chem. Phys 1973;58:1564.
30. Helfrich W, Harbich W. Chem. Scr 1985;25:32.
31. Kleinert H. J. Math. Phys 1986;27:3003.
32. Burkhardt TW. J. Phys. A: Math. Gen 1995;28:L629.
33. Odijk T. Biophys. Chem 1993;46:69.
34. Jain S, Nelson DR. Macromolecules 1996;29:8523.
35. In Ref. [25] short-range hydration forces were included in the harmonic approximation, but image-charge interaction and steric interactions were still neglected.
36. Odijk T. Macromolecules 1993;26:6897.
37. Kornyshev AA, Leikin S. J. Chem. Phys 1997;107:3656.
38. Philip JR, Wooding RA. J. Chem. Phys 1970;52:953.
39. Cherstvy AG, Kornyshev AA, Leikin S. J. Phys. Chem. B 2002;106:13362.
40. For purely steric interactions this approximation leads to a free energy $F_s = ck_BTL / D^{2/3}\left(l_p^b\right)^{1/3}$, where D is the effective diameter of the cylinder. From simulations [M. Dijkstra, D. Frenkel, H. N. W. Lekkerkerker, Physica A **193**, 374 (1993)], the value of the constant is $c = 2.46 \pm 0.07$. If we suppose that the confinement diameter is $D = 2(R_0 - 2a)$ and $\mu = 1/2$, we find $c \simeq 2.51$, in good agreement with the simulation results.
41. Feynman, RP. Statistical Mechanics (A set of lectures). Westview Press; New York: 1998.
42. Bogoliubov NN. Dokl. Akad. Nauk USSR 1958;119:244.
43. Katchalsky A. Pure Appl. Chem 1971;26:327.
44. Odijk T. Macromolecules 1983;16:1340.
45. Odijk T. Macromolecules 1986;19:2313.
46. Miklavic SJ. Phil. Trans. R. Soc. London A 1994;348:209.
47. Manning GS. J. Chem. Phys 1969;51:924.
48. Netz RR, Orland H. Eur. Phys. J. E 2003;11:301. [PubMed: 15011050]
49. Hsiao, C.; Tannenbaum, M.; Van Deusen, H.; Hershkovitz, E.; Perng, G.; Tannenbaum, A.; Williams, LD. Nucleic Acid Metal Ion Interactions. Hud, N., editor. The Royal Society of Chemistry; London: 2008. p. 1-35.
50. Odijk T. Europhys. Lett 1993;24:177.
51. For instance, an additional term, $\beta\,(d\mathbf{r}_{j,1}(z) / dz)^2$, may be introduced into our effective theory (Eq. (12)) to describe nematic aggregates in which we may no longer assume that $\bar{\psi} \ll 1$. Here β is the order parameter for nematic ordering [24].
52. At small surface-surface separations, factors like the discreteness of the solvent may become important.
53. Parsegian VA, Rand RP, Fuller NL, Rau DC. Methods Enzymol 1986;127:400. [PubMed: 3736427]
54. Yethiraj A. J. Phys. Chem. B 2009;113:1539. [PubMed: 19035818]
55. Basser PJ, Schneiderman R, Bank RA, Wachtel E, Maroudas A. Arch. Biochem. Biophys 1998;15:207. Arch Biochem Biophys. 1998 Mar 15;351(2):207-19. [PubMed: 9515057]
56. Elliott GF, Hodson SA. Rep. Progr. Phys 1998;61:1325.
57. Ateshian GA, Soltz MA, Mauck RL, Basalo IM, Hung CT, Lai WM. Transport in Porous Media 2003;50:5.
58. Rau DC, Parsegian VA. Biophys. J 1992;61:246–260. [PubMed: 1540693]
59. Podgornik R, Strey HH, Gawrisch K, Rau DC, Rupprecht A, Parsegian VA. Proc Natl Acad Sci USA 1996;93:4261. [PubMed: 8633052]
60. Ossawa, F. Polyelectrolytes. Marcel Dekker; New York: 1971.

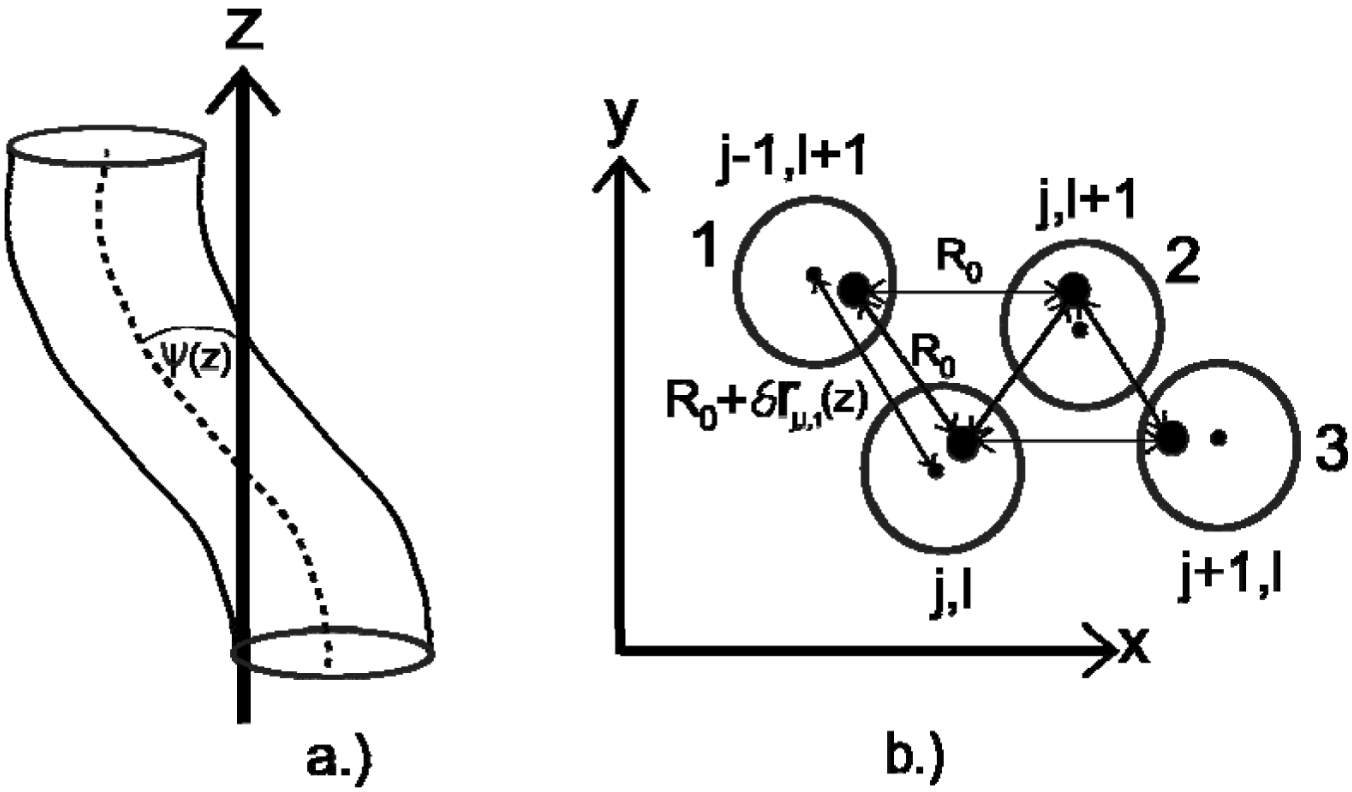

Fig.1.

Pictures denoting: **a.).** Of part of an undulating molecule with respect to the z-axis; the orientation of its mean major axis. The curved dotted line represents the fluctuating position of the molecular axis and $\psi(z)$ the tilt angle for one molecule is the angle the molecular axis makes with the z-axis. **b.)** A crossection of the undulating hexagonal lattice. The large dots are mean positions of the major axis of each molecule, which form the heaxagonal lattice with spacing R_0. The small dots indicate the actual positions of each molecular axis. The deviation of an axis from its mean value for a molecule sitting at site $\{j,l\}$ is given by $\mathbf{r}_{j,l}(S)$. For each nearest neighbour about $\{j,l\}$ is numbered from 1 to 6 with the index i. Then, each interaxial separation can be expressed as $R_0 + \delta r_{j,l,i}(z)$, where for instance the change in intexaxial separation $\delta r_{j,l,1}(z)$ of a molecule with respect to its nearest neibour $i = 1$ may be expressed as $\delta r_{j,l,i}(z) = |\mathbf{R}_{j-1,l+1} - \mathbf{R}_{j,l} + r_{j-1,l+1}(z) - r_{j,l}(z)| - R_0$, where $\mathbf{R}_{j,l}$ are the position vectors of each mean axis in the lattice.

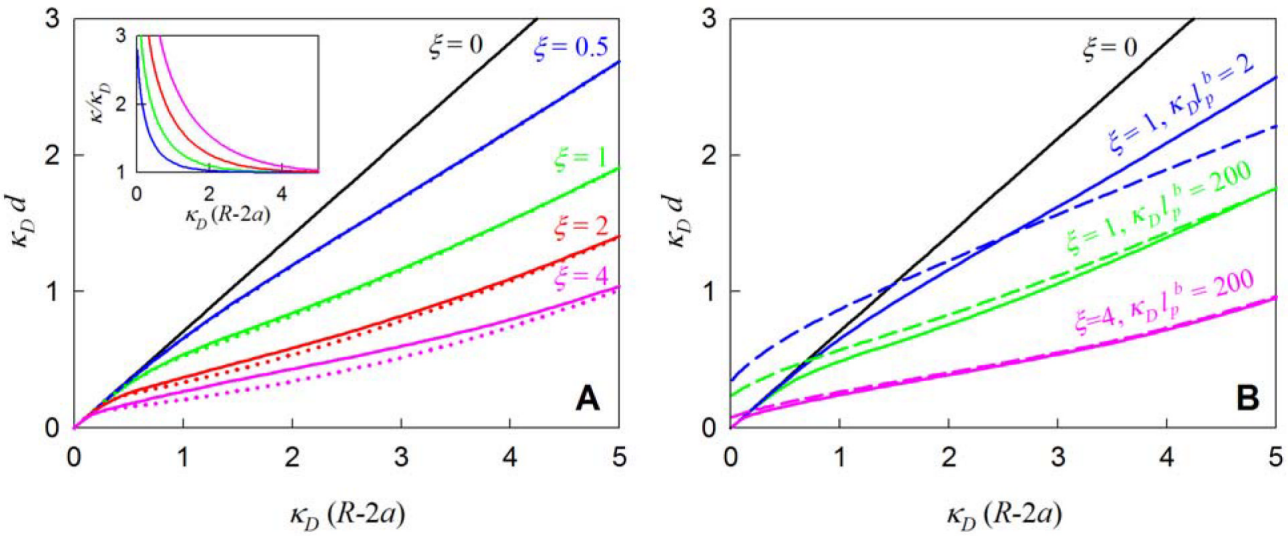

Fig.2.

Polyelectrolyte undulations in aggregates. **A.** Dependence of the rms undulation amplitude d on average surface separation between the molecules (R_0–2a) at different values of the renormalized Manning parameter $\xi = l_B / \tilde{l}_c$; calculated with κ self-consistently determined from Eqs. (6)–(8) (solid lines) and with $\kappa = \kappa_D$ (dotted lines). Although κ rapidly increases with decreasing surface separation (inset), the effect of this change in κ on the undulation amplitude is relatively minor even at large ξ. Line colors in the inset correspond to the same ξ as in the main panel. **B.** Undulation amplitude calculated within our model (Eq. (31), solid lines) and within the previously proposed [33] approximation for highly charged polyelectrolytes (Eq. (33), dashed lines). The following parameters were used for all calculations: $1/\kappa_D$ = 7 Å, a = 10.5 Å ($2\kappa_D a$=3). These values and $\kappa_D l_p^b$=71 $\left(l_p^b \approx 500 \text{ Å}\right)$ correspond to DNA in physiological saline.

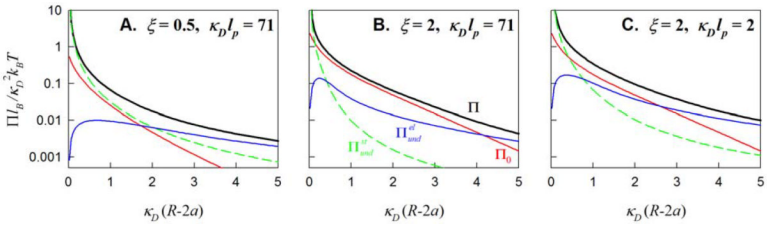

Fig 3.

Components of osmotic pressure in polyelectrolyte aggregates. Note that undulations are important both at large and small surface separations, shifting the whole osmotic pressure curve (Π) compared to the osmotic pressure in aggregates of straight, infinitely rigid rods ($=\Pi_0$). The calculations were performed with the same parameter values as in Fig. 2. Note that $\kappa_D^2 k_B T / l_B \approx 12$ MPa=120 bar at $\kappa_D^{-1} \approx l_B \approx 7$ Å.